Linearization of S-Parameter Cascading for Analysis of Multiple Reflections

Richard J. Allred [1,2] and Cynthia M. Furse [2]

[1] Signal Integrity Software, Inc. (SiSoft)
Maynard, MA 01754
richard.allred@gmail.com

[2] Department of Electrical and Computer Engineering
University of Utah, Salt Lake City, Utah, 84112, USA
cfurse@ece.utah.edu

Abstract — This paper develops a method to derive intuitive understanding of the root causes of reflective interference created by the many impedance discontinuities between the packages, PCBs and connectors. Scattering parameters are cascaded to describe the system response and linearized to analyze the multiple reflections. An upper error bound of the linearization is derived and is validated with Monte Carlo studies.

Index Terms — Inter-symbol interference (ISI), networks and circuits, scattering parameters, signal integrity, signal processing, transmission line matrix.

I. INTRODUCTION

Computer interconnect design has become a critical aspect of integrated circuit (IC) signal integrity, which has become more complex due to the exponential increase in on-chip computing bandwidth [1]. The simplest model of a computer interconnect includes only the wires that connect two ICs. More realistically, an interconnect includes packages that hold each IC, printed circuit board (PCB) transmission lines and vias (which transition between PCB layers) and connectors, as seen in Fig. 1. When the signal stream of 0's and 1's traverses the interconnect at very low data rate frequencies (kHz to low MHz), the interconnect features are much smaller than the wavelength, and the wires are typically modeled as simple delays. As the data rate increases, the interconnect model requires more fidelity that includes impedance mismatch, dielectric loss, skin effect and copper surface roughness. At today's data rates which can exceed 28 Giga-bits-per-second, it is typical to model transmission lines with 2D solvers [2]. Also, fine geometric features that were neglected at lower speeds, such as the PCB vias, must be accurately modeled, typically with 3D full wave FEM or FDTD solvers [3].

The transfer function for detailed high frequency interconnect models is found by cascading (combining in series) the individual transmission line and 3D model segments. This cascading process [5, 6] is excellent for quantifying the total behavior of the system but obscures the source of multiple reflections, in part because the cascading process is non-linear, as will be shown in this paper. Linearization will enable the separation of the transfer function into physically meaningful pieces that allow us to determine which system features contribute most to the multiple reflections. This then enables redesign to reduce those reflections and improve signal integrity.

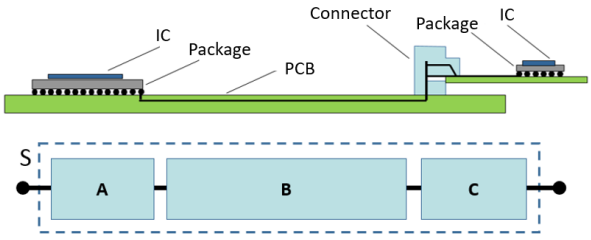

Fig. 1. Diagram of the 28G VSR computer interface [4] and an example of how the link can be modeled with three S-parameter segments: package (A), PCB (B), line card PCB (C). This interface is used in back-end servers for switching of internet traffic.

While others have addressed the need to identify and resolve reflective interference [7-9] the method described in this paper is, to our knowledge, the first rigorous process to do so. In lieu of a direct comparison of the proposed method with a traditional method, we will validate our method against Monte Carlo studies.

Section II discusses system level analysis and existing procedures for identifying sources of multiple reflections in a wired communication link such as the CEI 28G-VSR (very short reach) interface [4] shown in Fig. 1. Section III will describe an alternative to the standard ABCD matrix cascading approach, using

Submitted On: May 13, 2018
Accepted On: October 1, 2018

the analytic Mason's rule. Section IV derives the linearization of the cascading process. In Section V we derive an upper bound on the error introduced by the linearization and validate the bound with analytic and empirical Monte Carlo (MC) studies. Finally, we conclude with a discussion of the limitations of the proposed linearization, next steps and applications.

II. SYSTEM LEVEL ANALYSIS

Segments of an interconnect model such as those shown in Fig. 1 are usually represented by frequency domain scattering parameters (S-parameters):

$$\boldsymbol{S}(f) = \begin{bmatrix} S_{11}(f) & S_{12}(f) \\ S_{21}(f) & S_{22}(f) \end{bmatrix},$$

where $S_{ij}(f)$ is the complex voltage transfer function versus frequency between port j and port i [5]. $S_{11}(f)$ represents the reflective behavior looking into the input port 1, while $S_{21}(f)$ represents the through transfer function between the input port 1 and the output port 2. As it is understood that $\boldsymbol{S}$ is a frequency domain response, our notation will drop the explicit frequency reference. Also note that for passive and lossy interconnects considered here that $|S_{21}| = |S_{12}| \leq 1$, $|S_{11}| \ll 1$ and $|S_{22}| \ll 1$. This means that products of $\boldsymbol{S}$ matrix components will have magnitudes much less than 1.

The design of today's high speed interconnects for computer communication interfaces (e.g., PCIe4, 100G Ethernet) requires a careful budgeting of losses for long channels, as these can severely disperse and attenuate the signal [10]. Additionally, short channels can suffer from reflective interference caused by impedance discontinuities. These require an altogether different approach to resolve. While channel loss budgets are helpful for long channels, there is no similar reflection budget for short channels and their complicated multipath behavior. This paper proposes an approach to linearize the $\boldsymbol{S}$ matrix cascading process (the combining of $\boldsymbol{S}$ matrices together) which opens the door to innovative approaches for analyzing key features of reflective wired channels.

Consider the CEI 28G-VSR interface [4] shown in Fig. 1. This short channel can display highly reflective behavior from the impedance discontinuities at the package, PCB and connector junctions. To ensure that the transmitter and receiver circuit equalization schemes can overcome these channel and noise impairments, the design process uses a simulation of this environment. (Measuring multiple designs of the system would be too expensive and time consuming.) Figure 1 also shows an example of dividing the system into three segments which model the package (A), PCB (B) and connector with line card PCB (C). Each of these 2-port differential $\boldsymbol{S}$ matrices describes the frequency domain behavior of the segment and is obtained from either measurement, simulation (for example FEM or FDTD methods) [11], or empirical equations [12]. The segmentation of the system requires that the signal conductors at the boundary support TEM propagation and that any higher order modes have sufficiently attenuated [13].

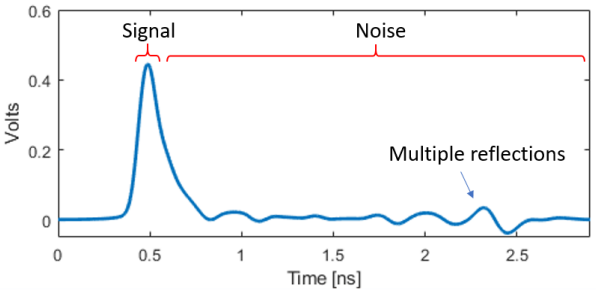

Fig. 2. Reflective noise can cause trouble for communication systems as can be seen by the pulse response of the system shown in Fig. 1. The energy from a single positive bit bounces around inside the system, and these multiple reflections show up much later than the desired signal. These stray voltages can interfere with later signals and could potentially corrupt the recovery of sent information.

System level analysis involves a simulator cascading the segments together into a total end-to-end $\boldsymbol{S}$ matrix for the system [6, 14], before converting to the time domain pulse response as shown in Fig. 2. This channel pulse response can then be used to combine with the transmitter and receiver equalization to determine the link's performance [15]. This analysis assumes that the $\boldsymbol{S}$ matrices are of good quality in that they are passive, causal and accurate [3, 16]. If they are not, numerical noise can propagate though the cascading process and corrupt the total end-to-end response.

This process of cascading segment models is excellent for quantifying the system performance but obscures the source of the multiple reflections, which makes redesigning to minimize them very difficult. To find the source of the multiple reflections in a system, the literature suggests a guess-and-check approach. The most common procedure is to consult the simulated time domain reflectometry (TDR) waveform to estimate where the largest impedance discontinuity is located [8]. Alternatively, the frequency domain insertion loss can be examined for problematic resonances whose frequencies are inversely proportional to the electrical length of the segment creating the reflective interference [17]. This section of the interconnect is then modified by removal or redesign to see if the system performance improves [7, 17]. When applied iteratively, this approach usually identifies the primary source of reflective interference. However, the process is not systematic or wholly repeatable due to the many subjective choices involved. Additionally, removing or modifying a segment of the system fundamentally changes the system. This makes

the true impact of a single discontinuity difficult to quantify. It is challenging to determine what to modify and how to modify it [7].

We would like to find a way to quantify how each ***S*** matrix segment contributes to the reflections in the total system response. Others have hinted at this goal [9], but we will demonstrate how to actually achieve this. Because the process of cascading ***S*** matrices is non-linear, a linearization or decomposition will be required to separate the transfer function into physically meaningful pieces. In this paper, we will apply the analytic Mason's rule to the ***S*** matrix cascading process and linearize this result. This will allow us to resolve the effects of reflections from individual segments of the system, thus enabling redesign to remove these effects.

III. MASON'S RULE

The usual approach to cascading a series of ***S*** matrices involves converting each ***S*** matrix to an ABCD matrix [5] or transmission matrix [6], multiplying the matrices together, and then converting back to ***S*** matrix form. The cascading process can determine the total system behavior, but it obscures how each segment contributes to the overall response. We propose an alternative approach, expressing the series of ***S*** matrices (for example three ***S*** matrices named **A**, **B** and **C**) as a signal flow graph, as shown in Fig. 3 (a), and then combining them with Mason's rule [18]. The signal flow graph is created by placing each ***S*** matrix's through responses (e.g., A_{21} and A_{12}) and reflection responses (e.g., A_{11} and A_{22}) as shown in Fig. 3 (a). Mason's rule provides an analytic solution (though non-linear) of the total system response. It also provides intuition into how reflective multipath behavior occurs in the system. A major insight is that pairs of impedance discontinuities form resonant loops (Fig. 3 (b)) which trap energy before returning it to the system. This delayed energy can eventually arrive at the receiver and may create an error in the bit decision.

The Mason's rule procedure to solve for the total S_{21} of the signal flow graph in Fig. 3 (a) is to first identify all forward paths. For our application, a forward path is one that starts on the left, ends on the right and does not circle back on itself; the only forward path in Fig. 3 (b) is $G_1 = A_{21}B_{21}C_{21}$. Second, identify the loops (paths that start and end at the same location) as shown in Fig. 3 (b) which are $L_1 = A_{22}B_{11}$, $L_2 = B_{22}C_{11}$, and $L_3 = A_{22}B_{21}C_{11}B_{12}$.

The next step is to identify the determinant (Δ) of the graph and the co-factor (Δ_i) of each path. The determinant, Eqn. 1, is found by collecting products of loop terms which do not touch. These products are taken one-at-a-time, two-at-a-time, three-at-a-time, etc. until all possible non-touching loop combinations are included. This calculation accounts for the interactions that occur between loops which do touch, and as will be seen below, a modification of this calculation opens the opportunity for linearization:

$$\Delta = 1 - \sum L_i + \sum_{non-touching} L_i L_j - \sum_{non-touching} L_i\, L_j L_k + \cdots. \quad (1)$$

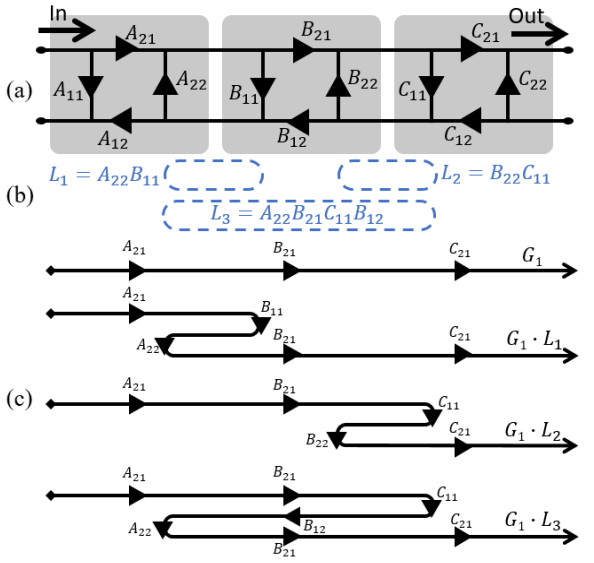

Fig. 3. (a) There are an infinite number of ways that energy can travel through a series of **S** matrix segments A, B, C in this signal flow graph. (b) Energy can resonate (get trapped) in the loops, L_1, L_2, and L_3. (c) Energy Transfer Diagram. A 1st order linearization of S_{21} is found by summing the possible paths through the signal flow graph. This includes the forward path $G_1 = A_{21}B_{21}C_{21}$ and all the paths going once through each of the loops in the system (or two bounces).

For our three-segment example, there are three one-at-a-time loops terms (L_1, L_2, L_3), one non-touching two-at-a-time loop term (L_1L_2) and no non-touching three-at-a-time loop terms. This results in the determinant of:

$$\Delta = 1 - L_1 - L_2 - L_3 + L_1L_2. \quad (2)$$

The cofactor of a forward path is defined as the determinant calculation over the set of loops which do not touch the forward path. Since the forward path G_1 touches all the loops, $\Delta_1 = 1$.

Once the paths, loops, determinant and cofactors are identified, Mason's rule provides a way to directly write down the transfer function equation:

$$G = \frac{\sum_k G_k \Delta_k}{\Delta}. \quad (3)$$

The Mason's rule process is summarized in Table 1. Finally, the total $S_{21}$of the signal flow graph in Fig. 3 (a) is:

$$S_{21} = \frac{A_{21}B_{21}C_{21}}{1 - L_1 - L_2 - L_3 + L_1L_2}. \quad (4)$$

Observe that the denominator collects the resonant behavior of the network and can significantly change with the inclusion of additional $\boldsymbol{S}$ matrix segments. This shows that the cascading of $\boldsymbol{S}$ matrices is a non-linear process, and the addition of more segments can significantly change the response.

While S_{21} could also be obtained through the ABCD or transmission matrix approach, the intuitive Mason's rule result provides insight into the physical behavior of the system. The linearization of this equation will decompose the response into a sum of physically meaningful terms which can then be analyzed individually to provide more insight into the causes of the reflective behavior of the system. This insight can be very useful in redesigning the system. The downside to the signal flow graph approach is that graphs which have many paths and many interacting loops can be very challenging to apply Mason's rule to by hand, and either simplifications to the structure or application of a matrix approach are required.

Table 1: Mason's rule analysis process summary

Step	Action
0	From a signal flow graph,
1	Identify desired input port and output port of network.
2	Identify all possible forward paths G_i between the input and output ports.
3	Identify all loops L_i in network.
4	Calculate the graph determinant: From the set of all loops, identify the combinations of loops which do not touch for groupings of two-at-a-time terms, three-at-a-time terms, etc. until all possible combinations are considered.
5	For each forward path G_i, calculate the cofactor Δ_i by identifying those loops which do not touch path G_i and then performing the determinant calculation over this set of loops.
6	Combine the forward paths G_i, cofactors Δ_i, and determinant Δ according to Eqn. 3 to obtain the transfer function between the input and output ports.

IV. LINEARIZATION DERIVATION

Our goal is to separate the expression for the total through response (S_{21}) of the system into a series of terms (visualized in Figs. 3 and 4) that can be analyzed individually so that we can identify which features are the most significant cause of multiple reflections. This decomposition or linearization is accomplished by simplifying Mason's rule to assume that all the loops are independent and do not touch each other. This leads to a denominator (i.e., the determinant, Δ, from Eqn. 1) that can be factored as shown in Eqn. 5 below:

$$S_{21} \approx \frac{A_{21}B_{21}C_{21}}{1 - L_1 - L_2 - L_3 + L_1L_2 + L_1L_3 + L_2L_3 - L_1L_2L_3}$$
$$S_{21} \approx \frac{A_{21}B_{21}C_{21}}{(1 - L_1)(1 - L_2)(1 - L_3)}. \quad (5)$$

Next, by applying the geometric series, $\frac{1}{1-x} = \sum_{n=0}^{\infty} x^n$ if $|x| < 1$, we can move the loop terms from the denominator to the numerator:

$$S_{21} \approx A_{21}B_{21}C_{21}\left(\sum_{n=0}^{\infty} L_1^n\right)\left(\sum_{n=0}^{\infty} L_2^n\right)\left(\sum_{n=0}^{\infty} L_3^n\right). \quad (6)$$

This expression can be further simplified by truncating the infinite series at $n = 1$ and discarding cross-terms which come from expanding the parentheses:

$$S_{21} \approx A_{21}B_{21}C_{21}(1 + L_1)(1 + L_2)(1 + L_3)$$
$$S_{21}^* = A_{21}B_{21}C_{21}(1 + L_1 + L_2 + L_3). \quad (7)$$

We call S_{21}^* the 1st order linearization of the through response S_{21}, and it shows how each resonant loop contributes to the total response. In the three-segment scenario, expanding the parentheses gives one forward path term and three loop terms which can be analyzed to determine which one is dominant. It is also the same expression that could be found by analyzing an energy transfer diagram and collecting all terms that have one loop (or two bounces), as shown in Fig. 3 (c). The utility of such a decomposition is that for signal integrity systems which suffer from high reflective interference, the impact of each loop response on the total system performance can be quantified [19].

The first order linearization for systems with more than three $\boldsymbol{S}$ matrix segments is generalized as:

$$S_{21}^* \approx (A_{21}B_{21}C_{21} \ldots)\left(1 + \sum L_i\right). \quad (8)$$

If the system has many large impedance discontinuities, significant energy can travel through more than one loop, and the 1st order linearization of S_{21} can be poor. To account for these additional multiple reflections, we return to the exact result of Eqn. 4 and bring the whole denominator to the numerator using the geometric power series relation:

$$S_{21} = \frac{A_{21}B_{21}C_{21}}{1 - L_1 - L_2 - L_3 + L_1L_2}$$
$$= A_{21}B_{21}C_{21}\left(\sum_{n=0}^{\infty}(L_1 + L_2 + L_3 - L_1L_2)^n\right). \quad (9)$$

Expanding the infinite series to $n = 2$ yields Eqn. 10 and discarding the terms with more than two loops (e.g., $L_1L_2^2$ and $L_1L_2L_3$) yields $S_{21}^{\ddagger}$, the 2nd order linearization shown in Eqn. 11. This is generalized for systems with more than three $\boldsymbol{S}$ matrix segments in Eqn. 12.

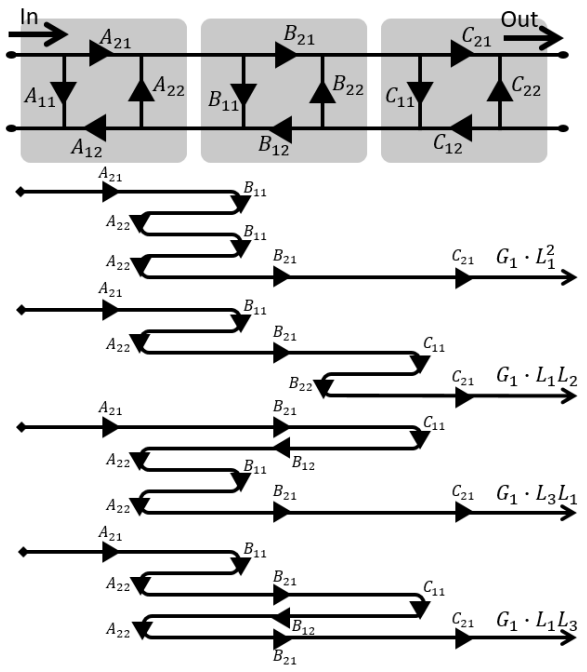

Fig. 4. Energy transfer diagram. The 1st order linearization of S_{21} can be improved (which we call the 2nd order linearization) by including all paths which travel through two loops (four bounces). Shown above are all such two loop paths which include the loop L_1. Additional two loop paths not shown are $G_1L_2^2$, $G_1L_3^2$, $G_1L_2L_3$ and $G_1L_3L_2$.

The energy transfer diagram in Fig. 4 provides an intuitive understanding of Eqn. 12 and shows that the 2nd order linearization can be found by augmenting the 1st order linearization with the energy transfer terms that contain two loops (or four bounces). It is interesting to note that the energy transfer terms $G_1L_3L_1$ and $G_1L_1L_3$ represent two separate ways to traverse the signal flow graph and therefore both must be included, thus the '2' coefficient in Eqn. 12 for touching loop terms.

For signal integrity systems of cascaded 2-port $\boldsymbol{S}$ matrices, the truncation of the infinite series at $n = 2$ is quite accurate as will be shown in the next section. For highly resonant systems, more terms may be needed. The linearization can be applied to differential, common, mode-conversion and single ended 2-port $\boldsymbol{S}$ matrices, depending on the desired application. The linearization is straightforward to calculate, as it only requires the determination of the primary loops and loops taken two-at-a-time. The Mason's rule response of these systems may be difficult to directly apply due to the many n-at-a-time loop combinations that must be considered. The numerical solution procedure of the linearization is summarized in Table 2 below.

Table 2: Linearization process summary

Step	Action
0	Diagram the signal flow graph for the network of 2-port S-parameters.
1	Calculate the forward path $\boldsymbol{G_1 = A_{21}B_{21}C_{21}}$ ...
2	Identify and determine the expression for each loop in the system, $L_1 = A_{22}B_{11}$, $L_2 = B_{22}C_{11}$, $L_3 = A_{22}B_{21}C_{11}B_{12}$, etc. For N segments, there will be $\frac{N(N-1)}{2}$ loops.
3	For 1st order linearization, calculate the loop responses by multiplying the forward path G_1 with each of the loops.
4a	For 2nd order linearization, determine the list of all two-at-a-time combinations of loops.
4b	For each combination determine if the two loops are touching in the signal flow graph.
5	Calculate the loop responses by multiplying the forward path response G_1 by each loop term.
	Single loop terms: $G_1 \sum L_i$.
	Single loop squared terms: $G_1 \sum L_i^2$.
	Non-touching terms: $G_1 \sum_{non-touching} L_i L_j$.
	Touching loop terms $2 \cdot G_1 \sum_{touching} L_i L_j$.
6	Calculate the linearization error.
6a	Find the true S_{21} by numerically cascading the S parameter segments [6].
6b	Calculate S_{21}^* or $S_{21}^{\ddagger}$ by summing the forward path with the loop responses.
6c	Calculate the error as the difference between S_{21} and S_{21}^* or $S_{21}^{\ddagger}$.

The linearization is useful as an insight into the reflective behavior of the system, but it can be computationally intense depending on the size of the system. For a system with N segments, the number of multiplication operations per frequency to cascade $\boldsymbol{S}$ matrices with the ABCD matrix approach is $O(26N)$, while to calculate the loop responses for the 1st order linearization is $O(N^3/3)$ and for the 2nd order linearization is $O(N^4/4)$ due to the exponential number of loops and combinations of loops to consider.

$$S_{21} = A_{21}B_{21}C_{21}\left(\begin{array}{c} 1 + \\ L_1 + L_2 + L_3 - L_1L_2 + \\ L_1^2 + 2L_1L_2 + L_2^2 + 2L_1L_3 + 2L_2L_3 + L_3^2 - L_1^2L_2 - L_1L_2^2 - L_1L_2L_3 + L_1^2L_2^2 \\ + \cdots \end{array}\right), \tag{10}$$

$$S_{21} \approx S_{21}^{\ddagger} = A_{21}B_{21}C_{21}(1 + L_1 + L_2 + L_3 \; + \; L_1^2 + L_2^2 + L_3^2 \; + \; L_1L_2 + 2L_1L_3 + 2L_2L_3), \tag{11}$$

$$S_{21}^{\ddagger} = (A_{21}B_{21}C_{21}\ldots)\left(1 + \sum(L_i + L_i^2) + \sum_{non-touching} L_iL_j \; + \; 2 \cdot \sum_{touching} L_iL_j\right). \tag{12}$$

V. ERROR ANALYSIS

As will be shown, the linearization error is proportional to the magnitude of the largest impedance discontinuity and the number of $\boldsymbol{S}$ matrix segments in the system. The relative error ratio, found by normalizing the error by the actual value, is evaluated, as it allows for extensive simplification. When applied to a three-segment system with 1st order linearization, the relative error ratio is:

$$\begin{aligned}
&\left|\left(S_{21} - S_{21}^{\ddagger}\right)\Big/ S_{21}\right| \\
&= \left|\frac{\frac{A_{21}B_{21}C_{21}}{1-L_1-L_2-L_3+L_1L_2} - A_{21}B_{21}C_{21}(1+L_1+L_2+L_3)}{\frac{A_{21}B_{21}C_{21}}{1-L_1-L_2-L_3+L_1L_2}}\right| \\
&= |1-(1-L_1-L_2-L_3+L_1L_2)(1+L_1+L_2+L_3)| \\
&= |L_1^2+L_2^2+L_3^2+2L_1L_2+2L_1L_3+L_2L_3-L_1L_2L_3 \\
&\quad -L_1^2L_2-L_1L2^2|.
\end{aligned} \tag{13}$$

Observe that all the single loop terms (i.e., L_1, L_2, L_3) of the simplified relative error ratio for the 1st order linearization cancel out, leaving only terms with products of two or more loops. Similarly, the simplified relative error ratio for the 2nd order linearization (not shown due to space considerations) includes only error terms composed of the products of three or more loops. To derive an upper bound on the error, we define $\nu = \max(|L_i|)$ and substitute ν for each loop in the relative error ratio. For *N*=3 segment and *N*=6 segment systems the 1st and 2nd order maximum error bounds are given in Table 3.

Table 3: Maximum error bound for linearization of order *O* for systems with *N* segments

N	***O***	**Maximum Error Bound**
3	1	$8\nu^2 - 3\nu^3$
3	2	$\boldsymbol{21\nu^3 - 8\nu^4}$
6	1	$190\nu^2 - 497\nu^3 + 411\nu^4 - 134\nu^5 + 15\nu^6$
6	2	$2353\nu^3 - 6239\nu^4 + 5186\nu^5 - 1695\nu^6 + 190\nu^7$

Figure 5 shows the 1st and 2nd order upper error bounds for a three-segment system as well as the 2nd order error bounds for the four-, five- and six-segment systems. This illustrates that the larger the loop terms (i.e., ν), the larger the error. Further, the more segments in the system, the more variability and thus the higher the upper error bound.

We will use an analytic MC study to validate this upper error bound. The exact S_{21} (Eqn. 4) and the 2nd order linearization (Eqn. 11), are calculated with $A_{21} = B_{21} = C_{21} = 1$ (representing a lossless system) and with random values of A_{22}, B_{11}, B_{22} and C_{11} which are calculated as follows. By noting that the diagonal S_{ii} terms of $\boldsymbol{S}$ are reflection coefficients, and by utilizing the reflection coefficient equation $\Gamma = \frac{Z_L - Z_1}{Z_L + Z_1}$ between a load impedance of Z_L and a line impedance Z_1, we relate the line impedance to the load impedance with the ratio r, $Z_1 = rZ_L$. This leads to $\Gamma = \frac{1-r}{1+r}$, which gives the reflection coefficient in terms of the ratio of impedance discontinuity, r. For the application of high speed interconnects, the manufactured characteristic impedance variation of mid-priced PCB transmission lines is typically +/- 15%. A conservative range for r is 0.5 to 1.5 which relates to an impedance variation of 50% to 150%. Therefore, each of the S_{ii} terms are calculated with the random variable r, drawn from the normal distribution $\mathcal{N}(1,0.15^2)$ which has approximately the range of 0.5 to 1.5. The results of the MC study are shown in Fig. 6. The upper error bound (given in Table 3) is not exceeded by 10^8 MC evaluations of the relative error ratio. Although not an absolute proof, this lends credibility to the upper bound calculation. The analytic MC study procedure is summarized in Table 4.

Table 4: Analytic MC validation of Error Bound for *N*=3 segments

Step	**Action**
0	Let $\boldsymbol{A_{21} = B_{21} = C_{21} = 1}$.
1	Calculate A_{22}, B_{11}, B_{22} and C_{11}.
1a	Select the ratio of impedance discontinuity, r, from $\mathcal{N}(1,0.15^2)$.
1b	Transform r to a reflection coefficient with $\Gamma = \frac{1-r}{1+r}$ and assign to return loss term.
2	Calculate the exact S_{21} from Eqn. 4.
3	Calculate the 2nd order linearization $S_{21}^{\ddagger}$ from Eqn. 11.
4	Calculate the relative error ratio.
5	Determine the max loop value, $\nu = \max(\lvert L_i \rvert)$.
6	Plot ν vs relative error ratio.

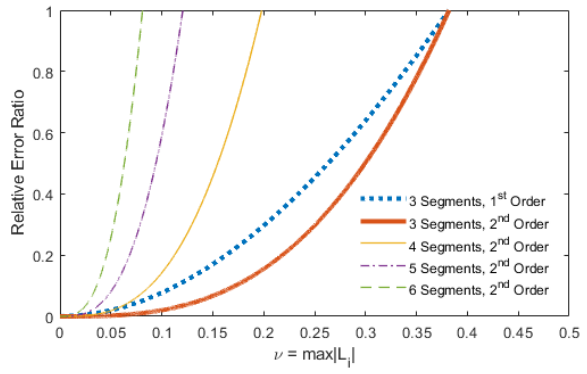

Fig. 5. The larger the impedance discontinuities in the system the larger the linearization error. The upper error bound is reduced by using the 2nd order linearization. The upper error bound is also dependent on the number of **S** matrix segments in the system, since each additional segment increases the number of loops or pairs of impedance discontinuities in the system.

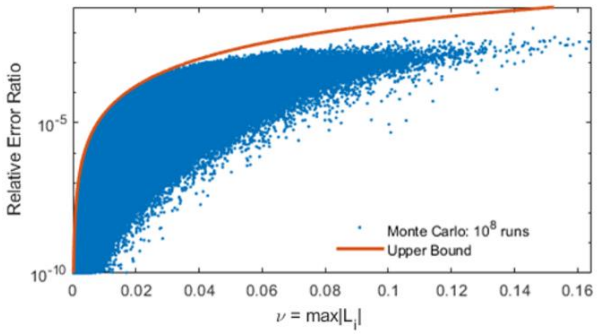

Fig. 6. 100 million MC runs validate the upper error bound for three **S** matrix segments with the 2nd order linearization of S_{21}. The solid line is the bound from Table 3 and the dots are Monte Carlo (MC) experiments.

An empirical MC study of the linearization error bound is accomplished by cascading transmission line $\boldsymbol{S}$ matrix models. These models were created using the IEEE 802.3bj 2-port differential transmission line model (TLM) equations [20] with parameter values from Table 5. These models are attractive to use, because they are readily available and are guaranteed to be causal by construction. The DC loss term is γ_0, a_1 is the attenuation and phase constant proportional to the square root of frequency, a_2 is the attenuation and phase constant proportional to frequency, and τ is the primary delay constant. Z_c is the differential characteristic impedance, and d is the transmission line length. The values of the behavioral attenuation and phase constants were obtained by the standards task force by fitting the equations to measured transmission line PCB data [21].

Table 5: IEEE 802.3bj 2-port differential Transmission Line Model (TLM) parameters

Parameter	Value	Units
γ_0	0	1/mm
a_1	1.734 x 10^{-3}	$ns^{1/2}$/mm
a_2	1.455 x 10^{-4}	ns/mm
τ	6.141 x 10^{-3}	ns/mm
Z_c	$U(60,140)$	Ω
d	$U(6,177)$	mm

The MC study entailed cascading N=3 and N=6 $\boldsymbol{S}$ matrix segments to evaluate the linearization error. In each case, each $\boldsymbol{S}$ matrix segment was obtained by using the parameter values in Table 5 and randomly selecting the characteristic impedance Z_c from a uniform distribution between 60 and 140 Ω and randomly selecting the length d from a uniform distribution between 6 and 177 mm. Care must be taken when selecting the frequency vector over which the TLM is created. Too coarse frequency sampling may lead to an incorrect phase delay of the TLM, while too fine frequency sampling will add unnecessary computation time with minimal improvement in accuracy.

For each experiment, the maximum error (over frequency) was determined, and ν was found as the maximum loop response, $\max(|L_1|, |L_2|, \ldots)$, at the frequency of the maximum error. The empirical MC study is summarized in Table 6.

Table 6: Empirical MC validation of error bound with transmission line for N=3 and N=6 segments

Step	Action
0	For each MC experiment,
1	Create transmission line $\boldsymbol{S}$ matrices from 1 to N.
1a	Randomly select $Z_c \in U(60,140)$ and $d \in U(6,177)$ and use parameter values from Table 5.
1b	Calculate $\boldsymbol{S}$ matrix through and reflection terms.
2	Calculate total S_{21} by cascading [6].
3	Calculate 2nd order linearization $S_{21}^{\ddagger}$ by following the procedure in Table 2.
4	Calculate the relative error ratio. Find the max error and the frequency it occurs at. Find $\nu = \max(\|L_i\|)$ at the max error frequency.
5	Plot max error vs. ν.

The results for the N=3 and N=6 $\boldsymbol{S}$ matrix segments MC study are shown in Fig. 7. We observe that for 1000 experiments the error bound is not exceeded. These studies further validate the upper error bound and show

some of the limitations of the linearization. Systems which have many large impedance discontinuities (greater than +/- 20% impedance mismatch) have large linearization error. Yet even in these situations, the linearization may still provide insight into the system and could still be the basis of useful analysis techniques.

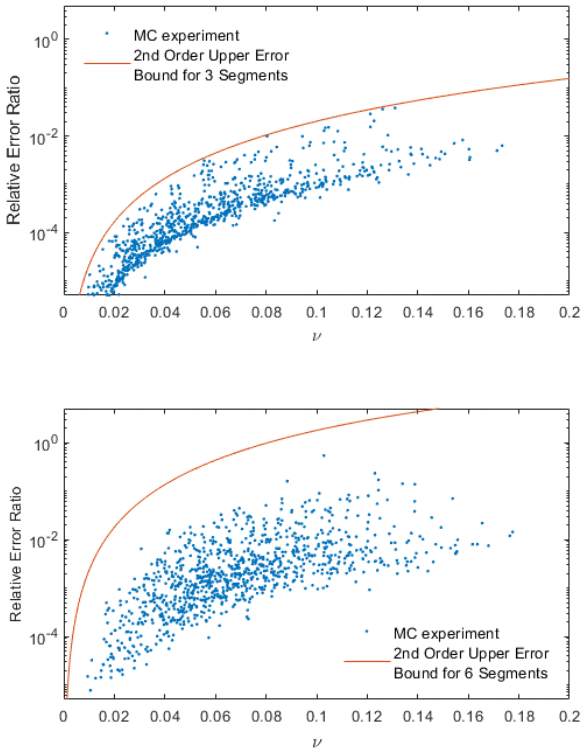

Fig. 7. The upper error bound holds for a realistic MC experiment from systems with three and six transmission line **S** matrix segments.

VI. CONCLUSION

To better analyze reflective multi-path behavior, this paper advocates the use of Mason's rule, as compared to the ABCD matrix approach, for the cascading of ***S*** matrix segments. This analytic formulation shows how resonant loops in the system give rise to reflective noise. A linearization or decomposition of this analytic formula allows for the independent analysis of physically meaningful terms to quantify how each resonant loop contributes to the overall multi-path behavior. An error bound is derived and shown to be dependent on the number of segments and the magnitude of the largest impedance discontinuities in the system. The error bound is validated with analytic and empirical MC studies. Overall, this linearization can yield more insight into the reflective behavior of complex systems and provide avenues to unique analysis techniques that will improve the design process of signal integrity interfaces or provide the capability to enable a reflective interference budgeting methodology.

The ***S*** matrix linearization method has been applied to optimizing a CEI 28G-VSR signal integrity interface [19, 22]. Here the first order linearization could successfully quantify the impact on receiver performance of each pair of impedance discontinuities.

Future work will explore applications of reflective interference budgeting for high-speed communication computer interfaces, sensitivity analysis of systems to catastrophic resonant behavior and interconnect optimization.

REFERENCES

[1] B. Casper, "Electrical interconnect potential and limits," in *Optical Interconnects Conference, 2014 IEEE*, 2014.

[2] T. Liang, S. Hall, H. Heck, and G. Brist, "A practical method for modeling PCB transmission lines with conductor surface roughness and wide-band dielectric properties," in *Microwave Symposium Digest, 2006. IEEE MTT-S International*, pp. 1780-1783, 2006.

[3] I. Bardi, E. Bracken, M. Commens, and R. Petersson, "Finite Element Method Practices to Result in Accurate and Causal Broad Band Frequency Sweeps in Simulating PCBs and Interconnects," *28th Annual Review of Progress in Applied Computational Electromagnetics*, 2012.

[4] "OIF2010.404.04: CEI-28G-VSR draft IA," 2010.

[5] D. M. Pozar, *Microwave Engineering*. John Wiley & Sons, 2009.

[6] J. Frei, X.-D. Cai, and S. Muller, "Multiport S-parameter and T-parameter conversion with symmetry extension," *IEEE Transactions on Microwave Theory and Techniques*, vol. 56, no. 11, pp. 2493-2504, 2008.

[7] D. Telian, S. Camerlo, K. Matta, M. Steinberger, B. Katz, and W. Katz, "Moving Higher Data Rate Serial Links into Production - Issues & Solutions," *Presented at the DesignCon 2014 Conference*, Santa Clara CA, 2014.

[8] D. Telian, S. Camerlo, M. Steinberger, B. Katz, and W. Katz, "Simulating Large Systems with Thousands of Serial Links," *Presented at the DesignCon 2012 Conference*, Santa Clara CA, 2012.

[9] C.-W. Huang, C. E. Smith, A. Z. Elsherbeni, and B. Hammond, "A novel simplified four-port scattering parameter model for design of four-pair twisted-pair cabling systems for local area networks," *IEEE Transactions on Microwave Theory and Techniques*, vol. 48, no. 5, pp. 815-821, 2000.

[10] W. T. Beyene, N. Cheng, and C. Yuan, "Design and analysis of multi-gigahertz parallel bus interfaces of low-cost and band-limited channels," in

Electrical Performance of Electronic Packaging, 2003.

[11] J. Lu and D. Thiel, "EMC Computer Modeling and Simulation Techniques," *22nd Annual Review of Progress in Applied Computational Electromagnetics*, 2006.

[12] H. Yordanov, M. T. Ivrlac, A. Mezghani, J. A. Nossek, and P. Russer, "Computation of the Impulse Response and Coding Gain of a Digital Interconnection Bus," *24th Annual Review of Progress in Applied Computational Electromagnetics*, 2008.

[13] M. Schneider, "Computation of impedance and attenuation of TEM-lines by finite difference methods," *IEEE Transactions on Microwave Theory and Techniques*, vol. 13, no. 6, pp. 793-800, 1965.

[14] "Quantum Channel Designer User Manual," *Signal Integrity Software, Inc.*, 2018.

[15] "I/O Buffer Information Specification (IBIS) Version 6.1.," 2015.

[16] P. Triverio, S. Grivet-Talocia, M. S. Nakhla, F. G. Canavero, and R. Achar, "Stability, causality, and passivity in electrical interconnect models," *IEEE Transactions on Advanced Packaging*, vol. 30, no. 4, pp. 795-808, 2007.

[17] Z. N. Yong, *et al.*, "Main cause of resonance appeared around 7.5 GHz on the frequency response of S-parameters of PWB," in *Electronic Packaging Technology and High Density Packaging (ICEPT-HDP), 2011 12th International Conference on*, 2011.

[18] S. J. Mason, "Feedback theory: Further properties of signal flow graphs," *Proceedings of the IRE*, vol. 44, no. 7, pp. 920-926, 1956.

[19] R. J. Allred, B. Katz, and C. Furse, "Ripple analysis: Identify and quantify reflective interference through ISI decomposition," in *Signal and Power Integrity (SPI), 2016 IEEE 20th Workshop on*, 2016.

[20] *IEEE Standard for Ethernet, Amendment 2: Physical Layer Specifications and Management Parameters for 100 Gb/s Operation Over Backplanes and Copper Cables*, IEEE Std 802.3bj-2014, 2014.

[21] "Proposal for a causal transmission line model," IEEE P802.3bj Task Force, http://www.ieee802.org/3/bj/public/mar14/healey_3bj_01_0314.pdf, March 2014.

[22] R. J. Allred, "System and method for signal integrity waveform decomposition analysis," U.S. Patent 9,633,164, issued April 25, 2017.

Richard J. Allred is a Principle Engineer at Signal Integrity Software, Inc. (SiSoft). He received his BS/MS in Electrical Engineering in 2006 from the University of Utah and is currently pursuing a Ph.D. in Electrical Engineering from the University of Utah.

He technically led Signal Integrity teams to design high speed graphics memory interfaces at Intel, contributed to the first 100 Gigabit Ethernet CMOS PHY at Inphi and provided software tool development and Tx/Rx IBIS-AMI models for SiSoft. He is a Member of IEEE and is currently researching how non-linear effects impact interconnect performance and performance estimation.

Cynthia M. Furse is the Associate Vice President for Research at the University of Utah and a Professor of Electrical and Computer Engineering. Furse received her B.S. in Electrical Engineering with a Mathematics minor in 1985, M.S. degree in Electrical Engineering in 1988, and her Ph.D. in Electrical Engineering from the University of Utah in 1994.

She has applied her expertise in electromagnetics to sensing and communication in complex lossy scattering media such as the human body, geophysical prospecting, ionospheric plasma, and aircraft wiring networks. She has taught electromagnetics, wireless communication, computational electromagnetics, microwave engineering, antenna design, and introductory electrical engineering and has been a leader in the development of the flipped classroom.

Furse is a Fellow of the IEEE and the National Academy of Inventors. She is a past AdCom Member for the IEEE AP Society and past chair of the IEEE AP Education Committee. She has received numerous teaching and research awards including the 2009 IEEE Harriett B. Rigas Medal for Excellence in Teaching. She is a Founder of LiveWire Innovation, Inc., a spin-off company commercializing devices to locate intermittent faults on live wires.